Available online at www.sciencedirect.com
ScienceDirect
Journal of Sound and Vibration 300 (2007) 126–138
JOURNAL OF SOUND AND VIBRATION
www.elsevier.com/locate/jsvi

A numerical method for moving load on continuum

C.G. Koh*, G.H. Chiew, C.C. Lim

Department of Civil Engineering, National University of Singapore, 1 Engineering Drive 2, Singapore 117576, Singapore

Received 11 February 2005; received in revised form 31 May 2006; accepted 24 July 2006
Available online 10 October 2006

Abstract

In this paper, a recently developed method called the moving element method is adopted for the dynamic analysis of half-space continuum under moving load. Plane strain condition is assumed and the continuum is discretised into "moving elements". These moving elements are not physical elements fixed to the continuum but are conceptual elements that "flow" with the moving load through the continuum. The method eliminates the need of keeping track the location of moving load relative to the element mesh. Numerical examples involving different load types such as strip load and concentrated load moving on half-space and layers on half-space are presented. The numerical results are verified against solutions obtained by alternative methods.

1. Introduction

Analytical methods were used in earlier research works to study moving load on continuum. Sneddon [1] first used Fourier integral transformation method to determine stress distribution in half-space due to the application of moving external pressure to its surface moving at subsonic velocity. Cole and Huth [2] extended the solution procedure to treat transonic and supersonic cases. Niwa and Kobayashi [3] further developed the method by considering other load types such as uniformly distributed and concentrated line loads acting normal or tangential to the surface of elastic half-space. Ang [4] and Payton [5] both considered the transient problem of a concentrated line load that suddenly appeared on the surface of the elastic half-space and subsequently moved at a constant speed. Eason [6] was one of the first few to solve a three-dimensional (3-D) moving load problem using Fourier integral transforms. Gakenheimer [7] and Norwood [8] considered 3-D transient problems of load applied suddenly to surface of elastic half-space and then moved at constant speed. Calladine and Greenwood [9] considered half-space as made of an incompressible elastic material whose modulus is linearly proportional to the depth from the free surface. By means of vertical particle displacement approximation, De Hoop [10] analysed the transient case of an initially stationary load which moved at subsonic or transonic speed on the surface of an elastic half-space. Jones and Petyt [11] studied transmission of vibration on the surface of an elastic isotropic and homogenous half-space subjected to harmonic load acting on a strip of finite width by means of dynamic stiffness matrix analysis. Sheng et al. [12] further considered

*Corresponding author. Tel.: +65 6874 2163; fax: +65 6779 1635.
E-mail address: cgkoh@nus.edu.sg (C.G. Koh).

0022-460X/$ - see front matter © 2006 Elsevier Ltd. All rights reserved.
doi:10.1016/j.jsv.2006.07.038

constant and oscillatory loads moving at constant velocity along a train track, and modelled the ground as several visco-elastic layers over an elastic half-space.

Although analytical methods give exact (or nearly exact) solutions, they are limited in practical applications due to the simplified geometry and conditions assumed. With the emergence of fast and low-cost computers, numerical methods such as the finite element method (FEM) are preferred. De Barros and Luco [13] evaluated the dynamic displacements of a multi-layered visco-elastic half-space subjected to a moving line load at constant velocity using Fourier synthesis of the frequency response. By means of Helmholtz decomposition and fast Fourier transform, Lefeuve-Mesgouez [14] investigated the transmission of vibration due to a moving harmonic strip load rigidly attached to the surface of an elastic half-space. In the study of half-space subjected to dynamic loads, Adam et al. [15] adopted both the FEM and boundary element method for 2-D problems. Kim et al. [16] proposed a similar hybrid approach to model the layered half-space. To reduce the integration range of wavenumbers in the fundamental solution, a semi-analytical approach was used.

A new numerical method called the moving element method (MEM) was proposed by Koh et al. [17] to solve train-track problems in the 1-D framework. By discretising the rail beam into conceptual elements that flow together with the moving train car, the proposed model eliminates the cumbersome need for keeping track of the vehicle or load position with respect to the track model. In this paper, the concept is extended to 2-D moving elements in order to study moving load on continuum.

2. Formulation of the MEM

In the context of plane strain modelling, consider a load moving at a constant velocity V on an elastic half-space as shown in Fig. 1. Let E, ρ and v be Young's modulus, density and Poisson's ratio, respectively, of the half-space. A fixed coordinate system (x, y) is defined. In the numerical model, the half-space is truncated and discretised into a finite number of moving elements as shown in Fig. 2. Elements marked with T are "typical" moving elements not in contact with the truncated boundary. Along the truncated boundary, infinite moving elements are required to simulate the zero displacement condition at infinity. They are denoted as side elements S1–S3, and corner elements C1 and C2 in Fig. 2. Each side element has one side mapping to infinity, and each corner element has two "infinity" sides.

The MEM tackles several shortcomings of the FEM in handling moving load problems. Firstly, instead of using the usual physical elements fixed to the continuum, moving elements are formulated in a coordinate system moving at the velocity of the load. The position of the moving load thus becomes fixed at a particular node in the moving element mesh, thereby avoiding the need to keep track of the loading point as required in the FEM. As the moving load is fixed in the moving element mesh, non-uniform mesh can be utilised where finer elements are used near the load and coarser elements further away. Secondly, the moving load will never reach the boundary end of the numerical model since the model travels along with it, and hence the solution will always be valid. Thirdly, the number of elements used in the MEM model is independent of the distance traversed by the load in the time duration considered. Hence, the MEM requires comparatively lesser elements and is more computationally efficient than the FEM does in general.

Quadrilateral eight-node (Q8) elements of the serendipity family are chosen in this study. All elements are mapped to a master element defined in the natural coordinates (ξ, η) system with nodal points numbered 1–8

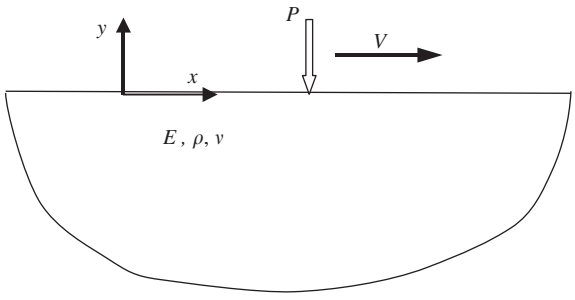

Fig. 1. Plane strain model for moving load problem.

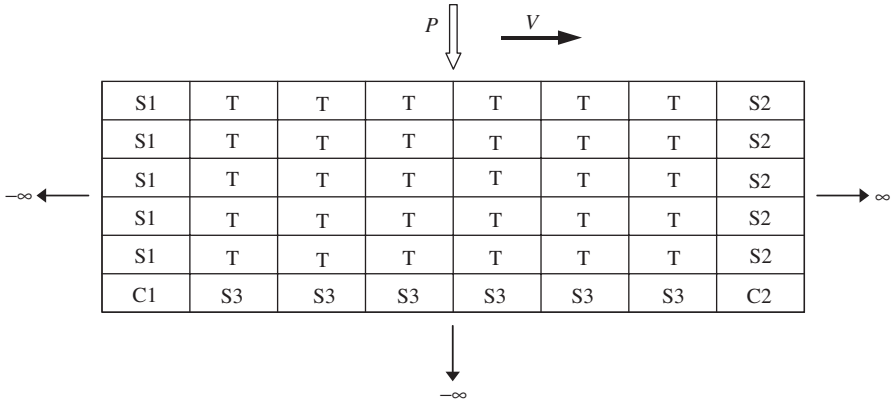

Fig. 2. Element types in the truncated half-space model.

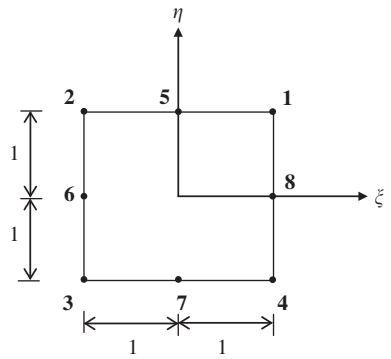

Fig. 3. Q8 master element in the natural coordinates system.

as shown in Fig. 3. Polynomial shape functionsfor the Q8 master element can be derived readily as

$$N_1 = \tfrac{1}{4}(1+\xi)(1+\eta)(-1+\xi+\eta);\ N_2 = \tfrac{1}{4}(1-\xi)(1+\eta)(-1-\xi+\eta),$$
$$N_3 = \tfrac{1}{4}(1-\xi)(1-\eta)(-1-\xi-\eta);\ N_4 = \tfrac{1}{4}(1+\xi)(1-\eta)(-1+\xi-\eta),$$
$$N_5 = \tfrac{1}{2}(1-\xi^2)(1+\eta);\ N_6 = \tfrac{1}{2}(1-\xi)(1-\eta^2),$$
$$N_7 = \tfrac{1}{2}(1-\xi^2)(1-\eta);\ N_8 = \tfrac{1}{2}(1+\xi)(1-\eta^2). \tag{1}$$

Using these shape functions, the displacements in the x- and y-directions, u_x and u_y, within each element are interpolated from the nodal displacements

$$\underline{u} = \underline{N}\ \underline{U}, \tag{2}$$

where $\underline{N}$ is a matrix containing the displacement shape functions,

$$\underline{N} = \begin{bmatrix} N_1 & 0 & N_2 & 0 & \cdots & N_8 & 0 \\ 0 & N_2 & 0 & N_2 & \cdots & 0 & N_8 \end{bmatrix} \tag{3}$$

and $\underline{U}$ is the nodal displacement vector,

$$\underline{U} = \left\{ u_{x_1} \quad u_{y_1} \quad u_{x_2} \quad u_{y_2} \quad \cdots \quad u_{x_8} \quad u_{y_8} \right\}^{\mathrm{T}}. \tag{4}$$

The mapping of various element types to the master element is illustrated in Fig. 4, where dashed lines indicate element sides mapped geometrically to infinity. For example, the left side of element S1 is mapped to $-\infty$ via $x = 2\xi a/(1+\xi)$; similarly for elements S2, S3, C1 and C2.

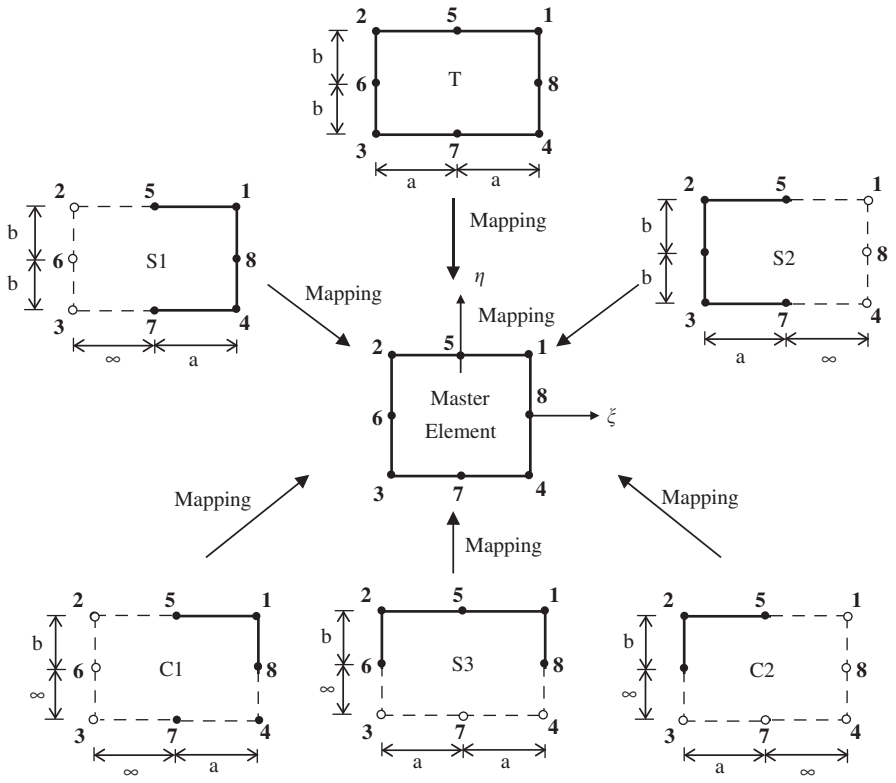

Fig. 4. Mapping of moving elements to master element.

By invoking the strain–displacement interpolation $\underline{\varepsilon} = \underline{B}\ \underline{U}$ where

$$\underline{B} = \begin{bmatrix} \frac{\partial N_1}{\partial x} & 0 & \frac{\partial N_2}{\partial x} & 0 & \cdots & \frac{\partial N_8}{\partial x} & 0 \\ 0 & \frac{\partial N_1}{\partial y} & 0 & \frac{\partial N_2}{\partial y} & \cdots & 0 & \frac{\partial N_8}{\partial y} \\ \frac{\partial N_1}{\partial y} & \frac{\partial N_1}{\partial x} & \frac{\partial N_2}{\partial y} & \frac{\partial N_2}{\partial x} & \cdots & \frac{\partial N_8}{\partial y} & \frac{\partial N_8}{\partial x} \end{bmatrix} \tag{5}$$

and the stress–strain relationship $\underline{\sigma} = \underline{D}\ \underline{\varepsilon}$, an expression for the stress at any point within the element is obtained in terms of the nodal displacements, i.e.

$$\underline{\sigma} = \underline{D}\ \underline{B}\ \underline{U}\,. \tag{6}$$

In the plane strain model, the elasticity matrix $\underline{D}$ is given as

$$\underline{D} = \frac{E(1-v)}{(1+v)(1-2v)} \begin{bmatrix} 1 & \frac{v}{1-v} & 0 \\ \frac{v}{1-v} & 1 & 0 \\ 0 & 0 & \frac{1-2v}{2(1-v)} \end{bmatrix}. \tag{7}$$

According to the principle of virtual work, for any compatible and small virtual displacements imposed on the body, the total internal virtual work done (W_I) must be equal to the total external virtual work done (W_E).

The internal virtual work can be expressed as

$$W_I = \overline{\underline{U}}^{\mathrm{T}} \left\{ \int_A \underline{B}^{\mathrm{T}} \ \underline{D} \ \underline{B} \, \mathrm{d}A \right\} \underline{U}, \tag{8}$$

where the over bar denotes the virtual system. Denoting the vectors for nodal forces, nodal velocities and nodal accelerations as $\underline{f}$, $\dot{\underline{U}}$ and $\ddot{\underline{U}}$, respectively, the external virtual work can be expressed as

$$W_E = \overline{\underline{U}}^{\mathrm{T}} \underline{f} - \int_A \overline{\underline{U}}^{\mathrm{T}} \underline{N}^{\mathrm{T}} \rho \, \ddot{\underline{U}} \, \mathrm{d}A. \tag{9}$$

To keep track of the load position, the moving coordinate system is defined as follows:

$$r = x - Vt, \tag{10}$$

where the origin of the r coordinate travels with the moving load at velocity V.

With the above coordinate transformation, we have the expressionsfor velocity and acceleration,

$$\dot{\underline{U}} = \frac{\partial u(x,t)}{\partial t} = -V \frac{\partial u(r,t)}{\partial r} + \frac{\partial u(r,t)}{\partial t}, \tag{11}$$

$$\ddot{\underline{U}} = V^2 \frac{\partial^2 u(r,t)}{\partial r^2} - 2V \frac{\partial^2 u(r,t)}{\partial r \, \partial t} + \frac{\partial^2 u(r,t)}{\partial t^2}. \tag{12}$$

Substituting Eq. (12) into Eq. (9) gives

$$W_E = \overline{\underline{U}}^{\mathrm{T}} \left\{ \underline{f} - \left[V^2 \int_A \underline{N}^{\mathrm{T}} \rho \underline{N}_{,rr} \, \mathrm{d}A \right] \underline{U} + \left[2V \int_A \underline{N}^{\mathrm{T}} \rho \underline{N}_{,r} \, \mathrm{d}A \right] \dot{\underline{U}} - \left[\int_A \underline{N}^{\mathrm{T}} \rho \, \underline{N} \, \mathrm{d}A \right] \ddot{\underline{U}} \right\}. \tag{13}$$

Rearranging Eq. (13) gives

$$\left[\int_A \underline{B}^{\mathrm{T}} \underline{D} \ \underline{B} \, \mathrm{d}A + V^2 \int_A \underline{N}^{\mathrm{T}} \rho \underline{N}_{,rr} \, \mathrm{d}A \right] \underline{U} - \left[2V \int_A \underline{N}^{\mathrm{T}} \rho \underline{N}_{,r} \, \mathrm{d}A \right] \dot{\underline{U}} + \left[\int_A \underline{N}^{\mathrm{T}} \rho \, \underline{N} \, \mathrm{d}A \right] \ddot{\underline{U}} = \underline{f}. \tag{14}$$

The above dynamic equation for the element can be expressed in the familiar form

$$\underline{K} \ \underline{U} + \underline{C} \ \dot{\underline{U}} + \underline{M} \ \ddot{\underline{U}} = \underline{F} \tag{15}$$

with the following equivalent mass, damping and stiffness matrices for the element:

$$\underline{K} = \int_A \underline{B}^{\mathrm{T}} \underline{D} \ \underline{B} \, \mathrm{d}A + V^2 \int_A \underline{N}^{\mathrm{T}} \rho \underline{N}_{,rr} \, \mathrm{d}A, \tag{16}$$

$$\underline{C} = -2V \int_A \underline{N}^{\mathrm{T}} \rho \underline{N}_{,r} \, \mathrm{d}A, \tag{17}$$

$$\underline{M} = \int_A \underline{N}^{\mathrm{T}} \rho \, \underline{N} \, \mathrm{d}A, \tag{18}$$

where $(\,)_{,r}$ denotes partial derivative with respect to r and $(\,)_{,rr}$ denotes second partial derivative with respect to r.

The load vector is defined as follows:

$$\underline{F} = \begin{bmatrix} f_{x_1} & f_{y_1} & f_{x_2} & f_{y_2} & \cdots & f_{x_n} & f_{y_n} \end{bmatrix}^{\mathrm{T}}, \tag{19}$$

where f_{x_n} is the nodal force in x-direction of nth node and f_{y_n} is the nodal force in y-direction of nth node.

To account for material damping, Eq. (17) can be revised as

$$\underline{C} = \underline{C}_{\mathrm{damping}} + 2V \int_A \underline{N}^{\mathrm{T}} \rho \underline{N}_{,r} \, \mathrm{d}A, \tag{20}$$

where, if Rayleigh damping is adopted,

$$\underline{C}_{\text{damping}} = a_0 \underline{M} + a_1 \underline{K}. \tag{21}$$

The element matrices are assembled in the usual way to form the corresponding system matrices (denoted by subscript S) for the half-space model considered, leading to the following equationsof motion:

$$\underline{K}_S \underline{U}_S + \underline{C}_S \dot{\underline{U}}_S + \underline{M}_S \ddot{\underline{U}}_S = \underline{F}_S, \tag{22}$$

where $\underline{F}_S$ contains many zeroes except at nodes where loads are applied. Since the loads travel with the moving elements, the loaded nodes will remain unchanged. Both transient and steady-state solutions can be obtained numerically by solving the above equations. For transient solution, step-by-step integration is required. It should be noted that, while the formulation is based on loads moving at constant velocity, the numerical method can be easily extended to deal with loads moving at varying velocity [17].

3. Numerical study

Table 1 summarises the five cases considered in the numerical study. The first four cases are studied for steady-state solutions, whereas the last case deals with a transient problem. All the MEM results are compared with available solutions. For steady-state cases corresponding to constant load travelling at constant velocity, the equation of motion (15) is elegantly reduced to the following equivalent static problem and solved easily by an equation solver:

$$\underline{K}_S \underline{U}_S = \underline{F}_S. \tag{23}$$

3.1. Point load moving on half-space (Case 1)

Consider a point load P travelling at 100 m/s on an elastic half-space. To compare with the analytical solution by Cole and Huth [2], the normalised vertical velocity at an observation depth is studied as defined below:

$$\dot{u}^* = \frac{\mu d}{PV} \dot{u}, \tag{24}$$

where μ is the shear modulus, d is the observation depth and P refers to the load applied (per unit length in the z-direction). To avoid comparing with singularity solution that exists in the analytical solution at the point of load application, the observation point is chosen at 10 m below point of load application.

The size of the moving element model is 60 m in the motion direction and 40 m in the depth direction. Uniform mesh is adopted for convergence study with three different element configurations: 20 (rows) × 18 (columns), 12 × 40 and 20 × 40. The number of rows is the number of elements used in the depth (vertical) direction, and the number of columns is the number of elements used in the motion (horizontal) direction. For illustration purpose, the normalised velocities obtained for the three different mesh sizes are compared in Fig. 5. As shown in Fig. 5, the error decreases with the use of more moving elements. The numerical results

Table 1
Summary of cases considered in the numerical study

Case	Load type (in plane strain model)	Load velocity (m/s)	Continuum	Alternative solutions for comparison
1	Point load	100	Half-space	Cole and Huth [2]
2	Strip load	400	Half-space	De Barros and Luco [13]
3	Strip load	400	A layer overlying half-space	De Barros and Luco [13]
4	Strip load	600	Five layers overlying half-space	De Barros and Luco [13]
5	Suddenly applied point load	100	Half-space	Ang [4]

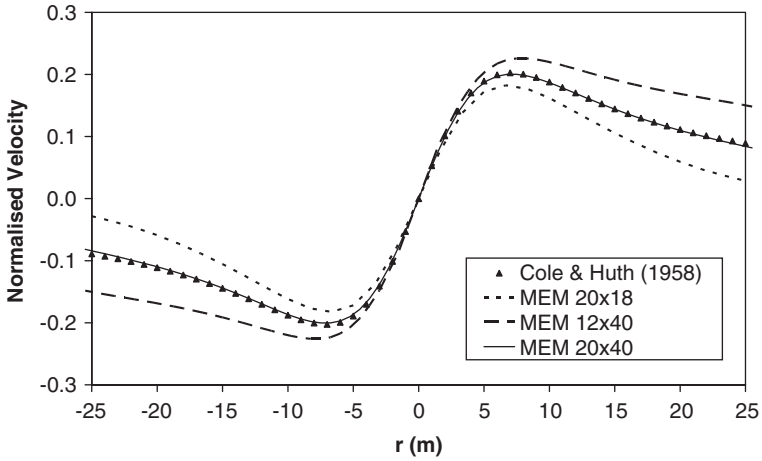

Fig. 5. Convergence with respect to element size for uniform mesh for Case 1.

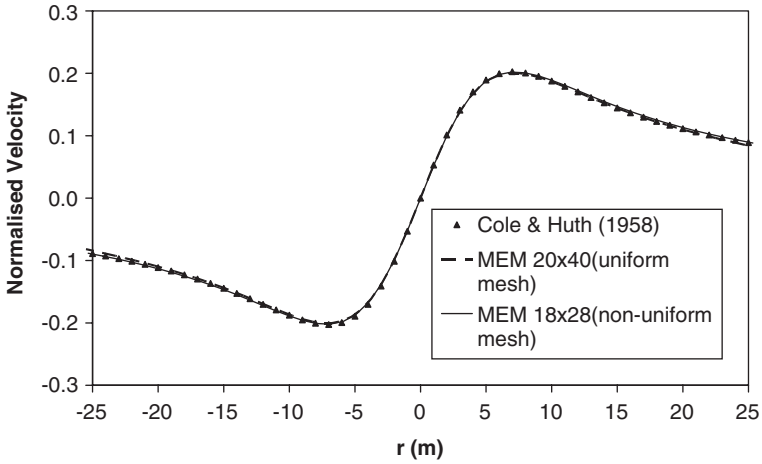

Fig. 6. Comparison of results based on uniform and non-uniform meshes for Case 1.

show that the MEM is in good agreement with the analytical solution when sufficient elements are used. The good agreement serves to validate the MEM 2-D formulation and computer program developed.

For better computational efficiency, non-uniform mesh should be used. A mesh of non-uniform elements can be generated such that refined elements are used where higher accuracy is required or where the solution varies sharply, e.g. in the vicinity of load point. Nevertheless, this is not possible in the FEM since the load moves across different elements at different times (unless re-meshing is carried out to follow the load location). In addition, the load point would move outside the refined region since the load moves relative to the finite elements. In contrast, the proposed MEM does not require re-meshing since the mesh is fixed in relation to the moving load. In this regard, a finer mesh can be used near the load and coarser mesh away. The row heights of the elements are varied by arithmetic progression as h, $h(1+r_h)$, $h(1+2r_h)$, … where the height of the topmost row is h and the height is increased by hr_h for each subsequent row. Similarly, the column widths are w, $w(1+r_w)$, $w(1+2r_w)$, …, beginning from the two middle columns and increasing progressively to both sides in a symmetric manner. The element configuration for the non-uniform mesh is 18×28 with initial dimensions $h = w = 1.937$ m and increment ratios $r_h = r_w = 0.0165$. The normalised velocity results are presented in Fig. 6, illustrating that the non-uniform mesh of 18×28 elements with considerably lesser elements yields about the same accuracy as the uniform mesh of 20×40 elements.

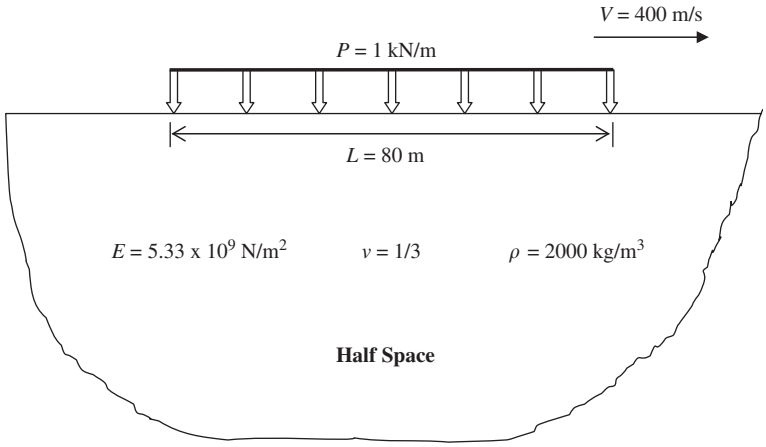

Fig. 7. Moving strip load on half-space (Case 2).

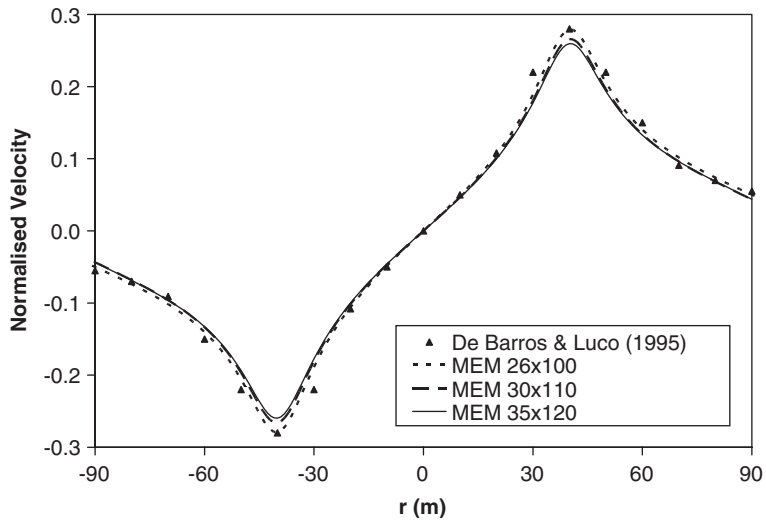

Fig. 8. MEM results based on three different meshes for Case 2 (strip load on half-space).

3.2. Strip load moving on half-space (Case 2)

Consider a uniform strip load P moving at 400 m/s on an elastic half-space, as illustrated in Fig. 7. The numerical solution given by De Barros and Luco [13] is used as the benchmark for comparison, for which the normalised vertical velocity $\dot{u}^*$ here is defined differently than Case 1:

$$\dot{u}^* = \frac{\mu d}{P c_S} \dot{u}, \tag{25}$$

where c_S is the shear wave velocity of the half-space. The observation point is defined at a depth (d) of 10 m below the midpoint of the moving strip load. In order to maintain a small column width near the two edges of the strip load, the column width (w) of all moving elements is kept constant. Based on a moving element model size of 150 m (depth) × 220 m (width), a convergence study is carried out for three element meshes, i.e. 26 × 100, 30 × 110 and 34 × 120 elements, by varying the height of first row, h. The row heights of elements are varied progressively according to $r_h = 0.15$. The normalised velocity at the observation point is plotted against the moving coordinate in Fig. 8. It is seen that the MEM results converge and are in good agreement with the solution obtained by De Barros and Luco [13].

Though elements with geometric mapping to infinity are used along the boundary of the truncated model, the numerical model is still an approximation for the half-space in general. To study the truncation effect of model size, three sizes are used: 115 m × 200 m, 147 m × 220 m and 182 m × 240 m. Based on a fixed element size with initial row height $h = 1.538$ m and element width $w = 2$ m, the normalised velocities are plotted against the moving coordinate in Fig. 9. The MEM results converge towards the numerical solution as the model size increases.

3.3. Strip load on a layer overlying half-space (Case 3)

The MEM can be applied to moving load on layered medium. As an illustration, consider a layer of 5 m depth overlying half-space with parameters as shown in Fig. 10. The strip load P spreading across width $L = 80$ m moves at 400 m/s, as considered by De Barros and Luco [13]. The normalised velocity $\ddot{u}^*$ at 10 m below the moving strip load is calculated according to Eq. (25), in which the shear velocity of the medium at the observation point is used.

As in the previous example, the column width is kept constant for strip load. The row heights of element are varied downwards according to arithmetic progression. Based on a model size of 133 m × 240 m, two different element sizes are studied by varying the numerical parameters: (a) $w = 1.81$ m (constant), $h = 1.07$ m and

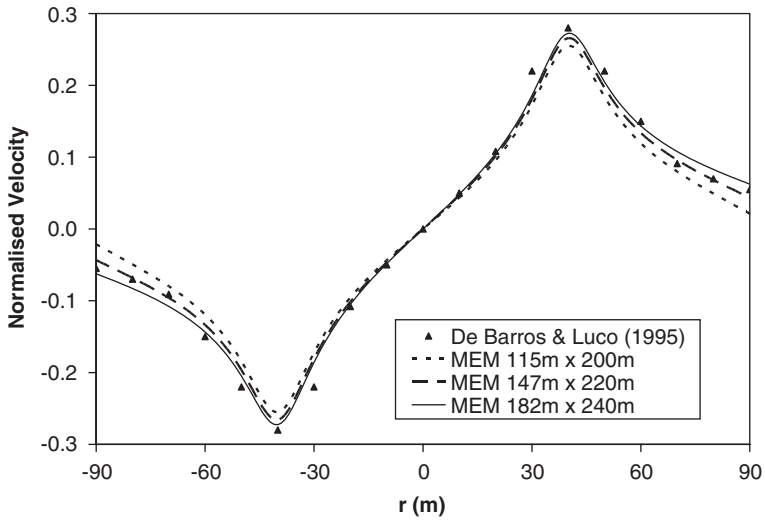

Fig. 9. MEM results based on three different model sizes for Case 2 (strip load on half-space).

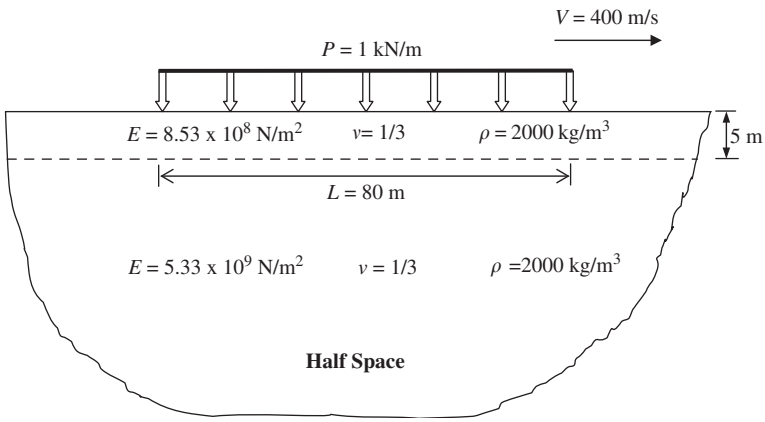

Fig. 10. Moving strip load on one layer overlying half-space (Case 3).

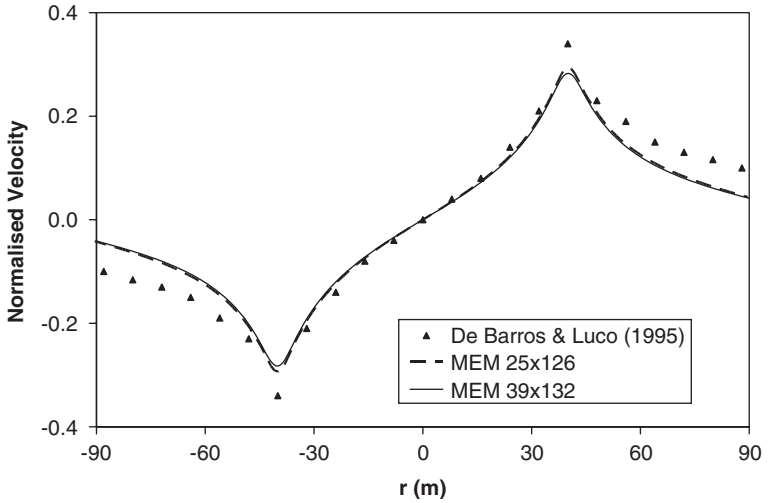

Fig. 11. MEM results based on three different meshes for Case 3 (one layer on half-space).

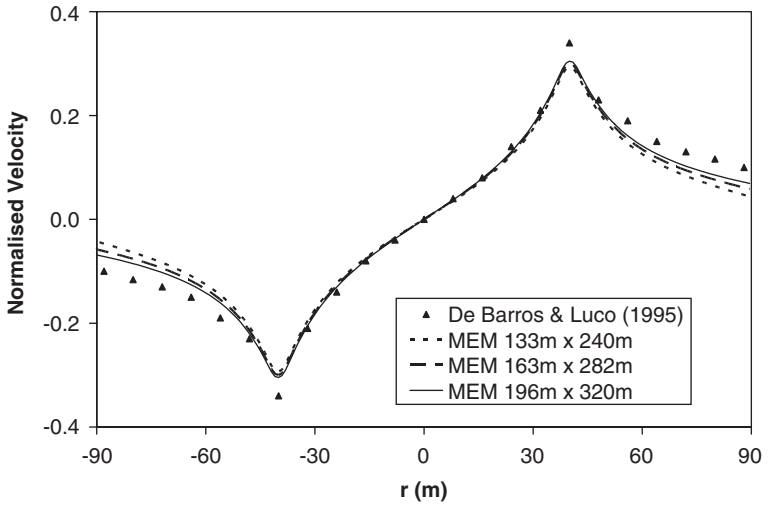

Fig. 12. MEM results based on three different model sizes for Case 3 (one layer on half-space).

$r_h = 0.11$; and (b) $w = 1.90\,\text{m}$ (constant), $h = 1.33\,\text{m}$ and $r_h = 0.25$. As shown in Fig. 11, the two different element meshes yield similar results which agree reasonably well with the numerical solution given by De Barros and Luco [13]. The discrepancy is not unexpected in view of the approximate nature of our solution and the solution by De Barros and Luco (both are obtained numerically).

The larger element size is used for the subsequent mesh-size convergence study. Using a fixed element size with $h = 1.33\,\text{m}$ and $r_h = 0.25$ and constant width of 2 m, a mesh truncation study is carried out with different mesh sizes of $133\,\text{m} \times 240\,\text{m}$, $163\,\text{m} \times 282\,\text{m}$ and $196\,\text{m} \times 320\,\text{m}$. The normalised velocities are again plotted against the moving coordinate (r) in Fig. 12. The MEM results converge towards the numerical solution as the model size increases.

3.4. Strip load moving on multi-layered half-space (Case 4)

As an extension of Case 3, consider a strip load (P) spreading across a width of 120 m and moving on a multi-layered half-space at constant velocity of 600 m/s. There are five layers of 1 m thick each overlying a stratum of stiffer material (half-space). All layers and the stratum have the same density of $2000\,\text{kg/m}^3$ and

Table 2
Material properties of five layers and stratum (half-space) used in Case 4

	Young's modulus, E (N/m^2)	Shear wave velocity (m/s)
Layer 1	2.13×10^8	200
Layer 2	1.20×10^9	475
Layer 3	2.43×10^9	675
Layer 4	3.63×10^9	825
Layer 5	4.56×10^9	925
Stratum	5.33×10^9	1000

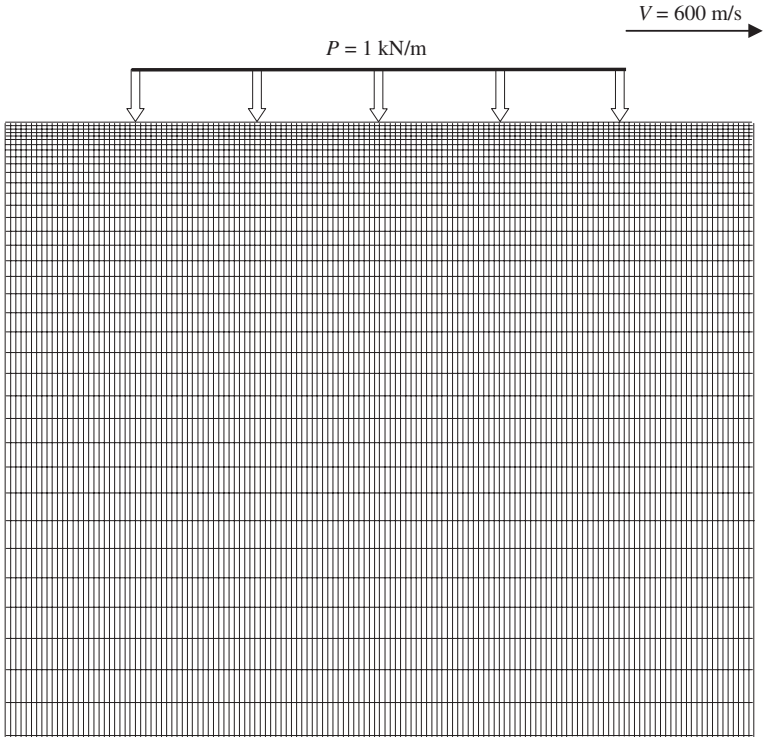

Fig. 13. Moving element mesh used in Case 4 (five layers on half-space).

Poisson's ratio of 1/3. Young's moduli and shear wave speeds are shown in Table 2. It is noted that the load speed of 600 m/s is larger than the shear wave speeds of the first two layers. The values of the normalised velocity $\dot{u}^*$ for an observation point 10 m below the moving strip load are calculated according to Eq. (29), in which the shear velocity of the underlying stratum at the observation point is used.

Similar to the previous cases for strip load, the element width (w) is kept constant and 1.5 m is used. Five element rows of 1 m height each are used to model the five layers above the stratum. For the stratum, non-uniform row heights are used according to $h = 1.39$ m and $r_h = 0.20$. The moving element mesh is depicted in Fig. 13. Three different model depths of 123, 176 and 219 m are studied, while the model width is kept constant at 220 m. The normalised velocity is plotted against the moving coordinate in Fig. 14. It is seen that the MEM results converge towards the numerical solution by De Barros and Luco [13] as the model depth increases.

3.5. Transient problem—suddenly applied moving load (Case 5)

To illustrate the feasibility of the MEM in tackling transient problems, consider a load $P = 1$ kN (per metre in the z-direction) that is suddenly applied at time $t = 0$ on the half-space at $x = 0$ and thereafter moving at

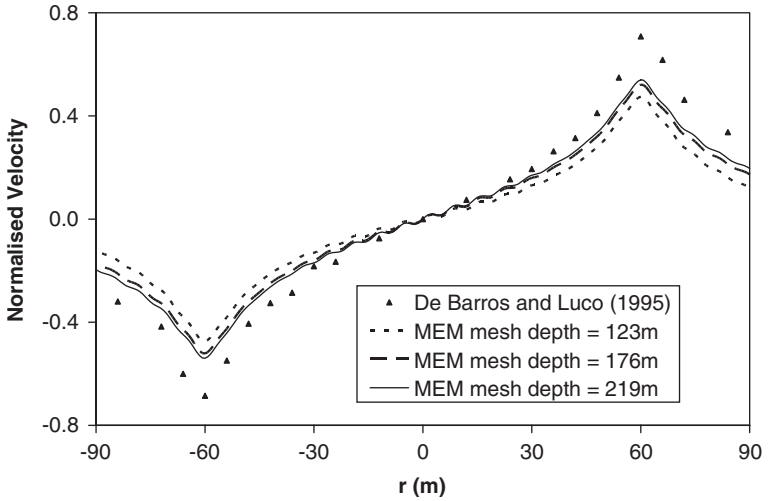

Fig. 14. MEM results based on three different mesh depths for Case 4 (five layers on half-space).

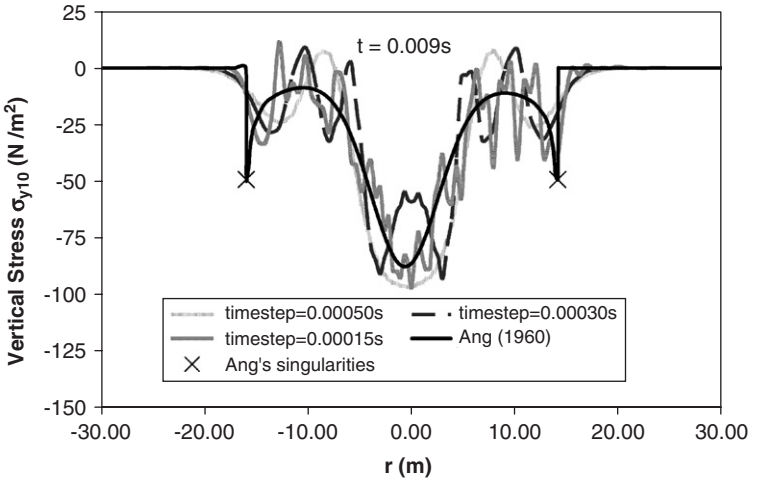

Fig. 15. Transient solutions for Case 5 (suddenly applied moving load).

100 m/s in the positive x-direction. The transient solution is obtained by numerically solving Eq. (22) in a step-by-step manner [17] and compared with the analytical solution obtained by Ang [4]. It should be noted that the analytical solution contains singularity in stresses.

Due to the sudden appearance of the load, the transient problem involves wave front propagation. Thus, very small time step and elements are required to capture the peak stresses associated with the arrival of wave fronts in the forward and backward directions. Based on a convergence study, the following mesh size is adopted: 45 m × 80 m with $w = 2.09$ m, $r_w = 0.075$ and constant element height of 1 m. Three time steps are considered: 0.00015, 0.00030 and 0.00050 s. Fig. 15 presents the results for the vertical stress (σ_{y10}) at 10 m below the point load at $t = 0.009$ s as an illustration. It is noted that, as the time step reduces, the numerical solution approaches the analytical solution, except for the two singularity points as marked by crosses in the figure.

4. Conclusions

In this paper, the MEM has been shown to be an elegant numerical method for solving 2-D moving load problems. By having elements moving with the load through the continuum, the MEM overcomes the

cumbersome task of tracking the load and the moving load will never reach the artificial boundary unlike in methods that use a fixed truncated domain for the half-space. The proposed method converts the steady-state moving load problem into an equivalent static problem which can be solved more efficiently than solving dynamic equations. It also facilitates the use of non-uniform mesh without the need of re-meshing. The five numerical examples illustrate the versatility and accuracy of the MEM in obtaining steady-state and transient solutions. The method can be easily applied to moving load problems in full space. Furthermore, while only plane strain model is considered here, the formulation can be readily modified to tackle moving load problems in plane stress and even 3-D frameworks.

References

[1] I.N. Sneddon, The stress produced by a pulse of pressure moving along the surface of a semi-infinite solid, *Rendiconti del Circolo Matematico di Palermo* 2 (1957) 57–62.
[2] J. Cole, J. Huth, Stresses produced in a half plane by moving loads, *Journal of Applied Mechanics* 25 (1958) 433–436.
[3] Y. Niwa, S. Kobayashi, Stresses produced in an elastic half-plane by moving loads along its surface, *Memoirs of the Faculty of Engineering Kyoto University* 28 (3) (1966) 254–276.
[4] D.D. Ang, Transient motion of a line load on the surface of an elastic half space, *Quarterly Journal of Applied Mathematics* 18 (1960) 251–256.
[5] R.G. Payton, Transient motion of an elastic half space due to a moving surface line load, *International Journal of Engineering Science* 5 (1967) 49–79.
[6] G. Eason, The stresses produced in a semi-infinite solid by a moving surface force, *International Journal of Engineering Science* 2 (1965) 581–609.
[7] D.C. Gakenheimer, J. Miklowitz, Transient excitation of an elastic half space by a point load travelling on the surface, *Journal of Applied Mechanics* 36 (1969) 505–515.
[8] F.R. Norwood, Exact transient response of an elastic half space loaded over a rectangular region of its surface, *Journal of Applied Mechanics* 36 (1969) 516–522.
[9] C.R. Calladine, J.A. Greenwood, Line and point loads on a non-homogeneous incompressible elastic half space, *The Quarterly Journal of Mechanics and Applied Methematics* XXXI (4) (1978) 507–529.
[10] A.T. De Hoop, The moving-load problem in soil dynamics—the vertical displacement approximation, *Wave Motion* 36 (4) (2002) 1–12.
[11] D.V. Jones, M. Petyt, Ground vibration in the vicinity of a strip load: a two-dimensional half space model, *Journal of Sound and Vibration* 147 (1) (1991) 155–166.
[12] X. Sheng, C.J.C. Jones, M. Petyt, Ground vibration generated by a load moving along a railway track, *Journal of Sound and Vibration* 228 (1) (1999) 129–156.
[13] F.C.P. De Barros, J.E. Luco, Stresses and displacements in a layered half space for a moving line load, *Applied Mathematics and Computation* 67 (1995) 103–134.
[14] G. Lefeuve-Mesgouez, D. Le Houédec, A.T. Peplow, Ground vibration in the vicinity of a high-speed moving harmonic strip load, *Journal of Sound and Vibration* 231 (5) (2000) 1289–1309.
[15] M. Adam, G. Pflanz, G. Schmid, Two- and three- dimensional modelling of half space and train-track embankment under dynamics loading, *Soil Dynamics and Earthquake Engineering* 19 (2000) 559–573.
[16] M.K. Kim, Y.M. Lim, W.Y. Cho, Three dimensional dynamic response of surface foundation on layered half space, *Engineering Structures* 23 (2001) 1427–1436.
[17] C.G. Koh, J.S.Y. Ong, D.K.H. Chua, J. Feng, Moving element method for train-track dynamics, *International Journal for Numerical Methods in Engineering* 56 (2003) 1549–1567.